Direct structural and spectroscopic investigation of ultrathin films of tetragonal CuO: Six-fold coordinated copper

Direct structural and spectroscopic investigation of ultrathin films of tetragonal CuO: Six-fold coordinated copper

D. Samal[1], Haiyan Tan[2(a)], Y. Takamura[3], W. Siemons[4], Jo Verbeeck[2], G. Van Tendeloo[2], E. Arenholz[5], C. A. Jenkins[5], G. Rijnders[1], and Gertjan Koster[1(b)]

[1] *MESA+ Institute for Nanotechnology, University of Twente - P.O. Box 217, 7500AE, Enschede, The Netherlands*
[2] *EMAT, University of Antwerp - Groenenborgerlaan 171, B-2020 Antwerp, Belgium*
[3] *Department of Chemical Engineering and Materials Science, University of California-Davis - Davis, CA 95616, USA*
[4] *Materials Science and Technology Division, Oak Ridge National Laboratory - Oak Ridge, TN 37831, USA*
[5] *Advanced Light Source, Lawrence Berkeley National Laboratory - 1 Cyclotron Rd, MS6R2100, Berkeley, CA 94720, USA*

Abstract – Unlike other $3d$ transition metal monoxides (MnO, FeO, CoO, and NiO), CuO is found in a low-symmetry distorted monoclinic structure rather than the rocksalt structure. We report here of the growth of ultrathin CuO films on $SrTiO_3$ substrates; scanning transmission electron microscopy was used to show the stabilization of a tetragonal rocksalt structure with an elongated c-axis such that $c/a \sim 1.34$ and the Cu-O-Cu bond angle $\sim 180°$, pointing to metastable six-fold coordinated Cu. X-ray absorption spectroscopy demonstrates that the hole at the Cu site for the CuO is localized in $3d_{x^2-y^2}$ orbital unlike the well-studied monoclinic CuO phase. The experimental confirmation of the tetragonal structure of CuO opens up new avenues to explore electronic and magnetic properties of six-fold coordinated Cu.

Introduction. – Understanding the atomic structure, chemical-bonding, and structure-property relationships in Cu-O coordinated compounds is one of the most intriguing problems in condensed-matter physics. Since the discovery of high-T_c superconductivity in the cuprates, interest in layered Cu-O alloys has been tremendous. Although no consensus exists yet on the theory of high-T_c superconductivity, clear experimental evidence for a strong antiferromagnetic super-exchange interaction (J) between the spins at the Cu sites is found to prevail in both the insulating parent phase and the doped superconducting phase [1–4]. This fact specifically motivates the study of novel layered Cu-O alloys that possess a higher J and that can eventually be used as a potential parent compound for high-T_c superconductivity. In this context, CuO with the rocksalt structure has recently drawn significant theoretical attention owing to its predicted high (up to

800 K) Néel temperature (T_N) [5,6]. The original proposal by Bednorz and Muller stated that oxides containing transition metal ions with partially filled e_g orbitals like Cu^{2+} will undergo strong Jahn-Teller (JT) distortion and consequently can have strong electron-phonon–interaction–based JT polaron model, possibly giving rise to superconductivity [7]. From the above considerations, a study of the highly symmetric cubic or tetragonal rocksalt CuO is of importance to elucidate the fundamental factors underlying high-T_c superconductivity in cuprates [8].

Despite the scientific interest around rocksalt CuO, the sole experimental demonstration involves the work by Siemons *et al.* [9] where ultrathin tetragonal CuO (t-CuO) films were grown on a $SrTiO_3$ (STO) substrate and their preliminary electronic properties were discussed. However, direct evidence for the crystal structure, chemical composition and the knowledge about the orbital occupation at the Cu site for the tetragonal CuO was missing. Our present findings based on scanning transmission electron microscopy (STEM), electron energy loss

---

(a)This author contributed equally to this paper.
(b)E-mail: g.koster@utwente.nl (corresponding author)

(EEL) spectroscopy and polarized X-ray absorption spectroscopy (XAS) provide this information and strongly corroborate the evidence for the tetragonal structure of ultrathin CuO layer. The structure of CuO as found in nature is unique and at variance with other $3d$ transition metal monoxides (TMMOs). While MnO, FeO, CoO, and NiO all crystalize in the rocksalt crystal structure (Fm-$3m$ space-group) with small lattice distortion ($< 2\%$) at low temperature [10–13], CuO crystalizes itself in a non-centrosymmetric monoclinic structure ($C2/c$ space-group, $a = 4.68373\,Å$, $b = 3.4226$, $c = 5.1288$ and $\beta = 99.54°$) [14,15] and, therefore immense attention has been drawn owing to its diversified characteristics: multiferroicity [2], orbital current [16], and low-dimensional magnetism [1,17]. From the magnetic point of view, CuO exhibits an electronic-correlation–induced insulating antiferromagnetic ground state similar to other TMMOs. However, it has two distinct antiferromagnetic phases: i) commensurate collinear and ii) incommensurate spiral structures with $T_N = 213\,K$ and $230\,K$, respectively [2]. While the other TMMO members with lower Z exhibit a linear trend of increasing T_N with increasing Z (MnO: $T_N = 118\,K$, FeO: $T_N = 200\,K$, CoO: $T_N = 291\,K$, and NiO: $T_N = 523\,K$) [13], the monoclinic CuO (m-CuO) shows a substantial departure from this trend. The reduction of T_N is believed to be related to the reduced effective $\boldsymbol{J}$ due to the lower Cu-O-Cu bond angle ($\varphi = 146°$) of the monoclinic structure. Since $\boldsymbol{J}$ strongly depends upon the Cu-O-Cu bond angle and can change from antiferromagnetic to ferromagnetic when φ changes from $180°$ to $90°$ [2]; one would expect that if CuO were found in the high-symmetry rocksalt structure or perhaps a closely related tetragonal structure with Cu-O-Cu bond angle ($\varphi = 180°$), then T_N would be enhanced. Since the interplay of superconductivity and magnetism is a key issue in the study of the physics of copper oxide systems, the high-symmetry phase of CuO with possible large antiferromagnetic coupling would be an ideal model system to investigate the correlated physics that lies at the heart of high-T_c cuprate superconductivity.

In this report, we have undertaken a detailed structural and spectroscopic investigation of ultrathin CuO films grown on STO substrates. The imposed epitaxial strain stabilizes a tetragonal rocksalt structure in ultrathin films with thicknesses $\leq$ 3–4 unit cells (uc). Our present results based on high-resolution STEM unambiguously demonstrate the existence of a high-symmetry tetragonal phase of CuO (where the Cu ion is six-fold coordinated to oxygen ions) with $c/a \sim 1.34$ (fig. 1(a)). Note that the observed c/a ratio for tetragonal CuO is comparatively smaller than what is generally found for the family of 2D layered cuprates, *e.g.* YBa$_2$Cu$_3$O$_{7-\delta}$. Since the Cu ion in the tetragonal geometry is surrounded by an elongated oxygen octahedron, it lifts the degeneracy associated with the e_g orbitals ($3d_{x^2-y^2}, d_{z^2}$) as schematically shown in fig. 1(c). This orbital configuration arises because the elongation of the c-axis lowers the Coulomb energy associated with

the electrons in the $3d_{z^2}$ orbital. Therefore, the hole ($Cu^{2+}(d^9)$) at the Cu site is expected to be localized at an $e_g d_{x^2-y^2}$ orbital for this novel phase, similar to what is generally observed in the case of high-T_c cuprate members. Using polarized XAS to selectively probe the $d_{x^2-y^2}$ and d_{z^2} orbitals, we clearly demonstrate the localization of the hole at the Cu site to the $3d_{x^2-y^2}$ orbital.

Experimental details. – The ultrathin CuO films were grown on TiO$_2$-terminated (001)-oriented STO substrates by pulsed laser deposition using a CuO target and at a pulse rate of $1\,Hz$, and a laser fluence of $2\,J/cm^2$. The substrate temperature was held at $650\,°C$ and the oxygen partial pressure was maintained at $0.3\,mbar$. Reflection high energy electron diffraction (RHEED) was used to monitor the growth process. After the deposition, the samples were cooled to room temperature in the deposition pressure at a controlled cooling rate of $10\,°C/$minute. The structural characterization of the samples was carried out by X-ray diffraction and high-resolution STEM, while composition analysis was performed by EEL spectroscopy and X-ray photoelectron spectroscopy (XPS). High-resolution high-angle annular dark-field (HAADF), annular bright field (ABF) STEM images and EEL spectra were acquired using the Qu-Ant-EM microscope at the University of Antwerp, which is a FEI Titan^3 80–300 equipped with a double aberration corrector and operated at $300\,KV$. Using a focused ion beam, thin cross-section lamellae of the films along two different directions were prepared for STEM investigation. In order to avoid any damage to the ultrathin CuO film during ion beam processing, it was capped with 20 uc of crystalline STO. The spatial resolution of the STEM images is $1\,Å$ and the energy resolution of the EEL spectra is $1.1\,eV$. The convergence and collection angle for HAADF STEM images and EEL spectra are 20 and $120\,mrad$, respectively. The ABF/ADF images were obtained simultaneously with an annular detector capturing scattering from 15 to 24 and from 26 to $60\,mrad$, respectively. An ABF/ADF elastic scattering image simulation was performed by the STEM-SIM software mimicking the experimental condition [18].

X-ray absorption spectra were acquired at beamline 4.0.2 at the Advanced Light Source (ALS) in total electron yield mode by monitoring the sample drain current. The linearly polarized X-rays were incident upon the sample with a $60°$ angle relative to the sample normal, and the $\boldsymbol{E}$ vector was applied either in-plane or at a $30°$ angle relative to the sample normal. To avoid charging effects during the measurement, the CuO layers were grown on Nb-doped (0.05% at.) STO substrates. Different STO capping layers were also investigated, but they did not significantly affect the measurement.

Results and discussion. – *In situ* monitoring of the growth of the CuO films using RHEED demonstrates a transition of the film structure as the film thickness increased. In the initial part of the growth, we clearly observe a RHEED pattern with elongated spots and not
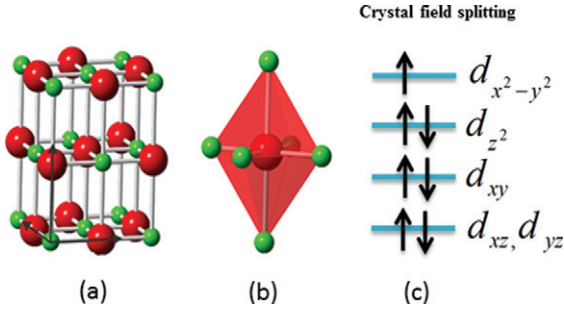
Fig. 1: Schematics for (a) the structure of ultrathin tetragonal CuO film ($a = 3.91(2)\,$Å and $c = 5.25(10)\,$Å) grown on STO. The green and red spheres represent oxygen and copper atom positions, respectively, (b) elongated CuO_6 octahedron surrounding Cu ion and (c) relevant tetragonal crystal field split energy levels with electronic occupation of d orbitals at the Cu site (d_{xz} and d_{yz} shown as degenerate).
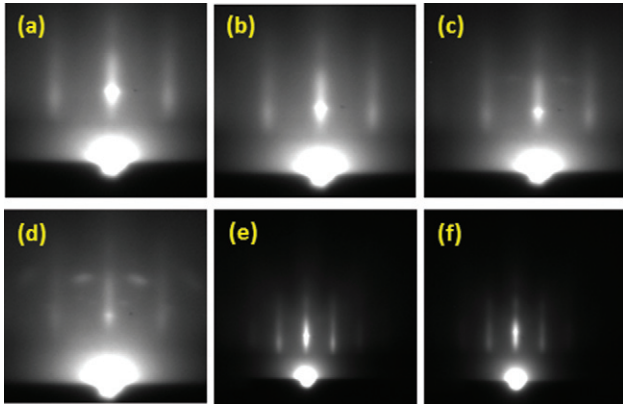

Fig. 2: Evolution of the RHEED pattern ((a)→(b)→(c)→(d)) during the growth of CuO on STO that clearly shows the transition from a streaky pattern ((a) and (b)) to the onset of 3D spots ((c) and (d)); (a), (b), (c) and (d) correspond to the RHEED pattern after ∼ 3, 4, 5 and 8 uc of CuO growth, respectively. A clear streaky RHEED pattern (e) at 650 °C after the growth of a tetragonal film (∼ 4 uc) and (f) after it is cooled down to room temperature.
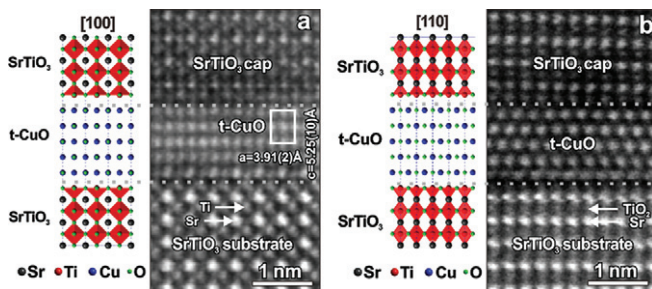

Fig. 3: HAADF-STEM images along the (a) [100] and (b) [110] direction. A tetragonal structure model matching the observations is shown on the left side of both figures.

showing reflections characteristic for 3D islands (fig. 2(a) and (b)), which corresponds to the tetragonal structure of CuO [9]. However, as the growth continued, 3D
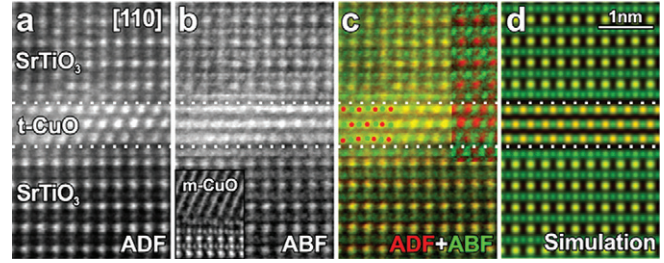

Fig. 4: (a) ADF image from the interface region showing the atomic columns of the heavy atoms along the [110] direction (Sr, Ti, Cu). (b) The reversed ABF image acquired simultaneously with the ADF image in (a) showing the atomic columns of light elements (oxygen) together with those of heavy elements. The inset shows a reversed ABF image of a thicker CuO film on the STO substrate. It has collapsed to its ordinary monoclinic structure which is clearly different from the tetragonal structure of ultrathin CuO film. (c) Combined color map with ADF in red and reversed ABF image in green. The heavy-element columns were combined to be yellow after color mixing while the O columns remain green. The inset is a combined color map with the ADF image in red and oxygen-enhanced ABF image in green, where the heavy elements (Cu/Ti/Sr) and light element (O) positions can be retrieved by Gaussian peak fitting (FWHM = 0.13 nm), respectively. The retrieved Cu and O positions are illustrated with red and green disks on the left of the CuO layer. The average Cu-O-Cu bond angle is 180 ± 2 degree estimated from measuring 30 Cu columns in the t-CuO horizontal planes. (d) Simulation of the ADF and the reversed ABF images.
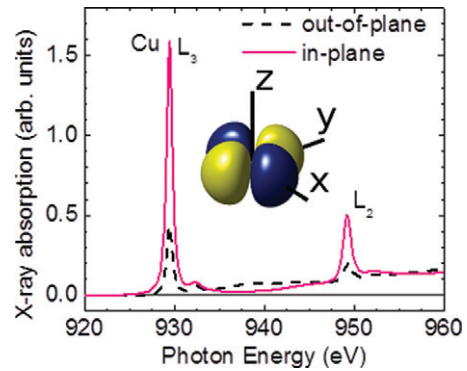

Fig. 5: Polarized XA spectra for a tetragonal CuO film. The inset shows the schematic for the $d_{x^2-y^2}$ orbital where the hole at the Cu site is preferentially localized.

spots gradually appear (fig. 2(c) and (d)), which are presumed to emerge when the film relaxes to the monoclinic phase. In most cases, elongated RHEED patterns were observed when the thickness of the CuO films was limited to 3–4 unit cells as monitored by RHEED oscillations. The elongated streaky 2D pattern at the growth temperature (fig. 2(e)) was retained upon cooling to room temperature (fig. 2(f)), demonstrating the stable nature of the ultrathin tetragonal CuO films. In order to ensure the growth of a pure CuO phase without the formation

of other copper oxide phases (*e.g.*, Cu_2O, Cu_3O_4), we have examined the structural and Cu valence state information using X-ray diffraction and XPS respectively. The results obtained from both the techniques confirm the growth of CuO phase; where Cu is in +2 state unlike in Cu_2O [9,19].

Detailed STEM was carried out to provide further insight into the structure of the ultrathin CuO film [20]. In order to investigate the three-dimensional arrangement of Cu cations, a representative sample with 2.5 uc thickness was prepared along the [100] and [110] directions. Figure 3(a) shows a HAADF-STEM image of the sample prepared along the [100] direction, in which the atomic columns of the heavy elements (*e.g.*, Cu, Ti, Sr) show up as bright spots. The middle CuO layer grows epitaxially with respect to the STO substrate with an atomic arrangement consistent with the projection of the rocksalt structure shown schematically on the left side of fig. 3(a). Using the lattice parameter of the STO substrate ($a = 3.905$ Å) as an internal calibration, we find the a-axis lattice parameter of CuO to be 3.91(2) Å, which matches well with that of the STO substrate and the capping layer. The c-axis lattice parameter of the CuO film is derived to be 5.25(10) Å. These observations suggest that the CuO layer stabilizes in an elongated rocksalt structure. HAADF-STEM of the sample prepared along the [110] direction shows that the CuO film has a hexagonal arrangement of atomic columns, in agreement with a tetragonal CuO structure as shown by the schematic on the left side of fig. 3(b).

The oxygen positions, which are equally important for the crystal symmetry determination, cannot be visualized by HAADF-STEM imaging due to the fact that oxygen has a much lower atomic number and cross-section for inelastic scattering. As an alternative, ABF-STEM is sensitive to both light (*e.g.*, oxygen) and heavy atoms (*e.g.*, Cu) in the structure and thereby provides crucial information on the oxygen ion positions [21]. Therefore, the combination of both ABF-STEM and ADF-STEM, provides a unique opportunity to simultaneously monitor the position of the oxygen atoms with respect to the Cu atoms [22]. Figure 4(b) shows a simultaneously acquired ABF image (intensity inverted to make the atoms appear as white spots on a dark background) together with its ADF image (fig. 4(a)) of the CuO film and its neighboring STO layers. Comparing the ADF and ABF images, extra oxygen atomic columns are clearly observed between two Ti columns in the ABF image of STO film in fig. 4(b). This proves that the spatial resolution at this experimental setting is capable of resolving the columns of oxygen ions from their neighboring Ti ions 1.4 Å away. Indeed, the ABF image corresponding to the CuO layer has extra columns belonging to the oxygen positions lying between two Cu columns. To improve the visibility of the oxygen columns, the intensity-inverted ABF image (in green) is superimposed with the ADF image (in red). The columns containing heavy elements (*e.g.*, Sr, Cu and Ti) together with oxygen ions are visible as yellow (overlay of red and green) dots whereas the columns containing only oxygen ions are visible in green. We clearly observe the presence of oxygen columns between the heavy Ti columns in the STO layer and between the heavy Cu columns in the CuO layer. This fact directly confirms the arrangement of the oxygen ions in the CuO layer as an elongated rocksalt structure as illustrated in fig. 1(a). Since the ABF images contain the information of both the heavy and light elements and the ADF only contain that of the heavy elements, the ABF image can be divided by its corresponding ADF image to enhance the visibility of the light elements further. This divided image (in green) was combined again with the ADF image (in red) (fig. 4(c), inset), which nicely shows the light atomic columns in green and the heavy ones in red. With such clearly identified oxygen columns, the average O-Cu-O bond angle is estimated to be 180 ± 2 degree. This result directly proves that both Cu and O ions adopt their corresponding atomic positions as demonstrated by the elongated rocksalt structure in fig. 1(a) for an ultrathin CuO layer. The simulated image assuming the structural model agrees well with the experimental result as shown in fig. 4(d). In order to confirm the chemical composition of the CuO and STO layers in a direct manner, EEL spectroscopy was performed and that confirms the designed film structure with negligible inter-diffusion.

XAS measurements were used to probe the electronic structure and symmetry of the unoccupied Cu $3d$ states for this novel phase of CuO. In these measurements, electrons are excited from a selected core shell to an empty valence state upon the irradiation of X-rays with the appropriate resonance energy. Since the orientation of the p and d orbitals are not spherically symmetric in space, the probability of an electron transition strongly depends on the orientation of the $\boldsymbol{E}$ vector of the linearly polarized X-rays with respect to the CuO_6 octahedra and therefore, the film's crystalline axes. Furthermore, the transition intensity scales with the number of empty states in the orbital being probed [23]. Therefore, using vertically or horizontally polarized X-rays oriented along the in-plane [100] direction (*i.e.*, the $\boldsymbol{E}$ vector aligned along the in-plane [010] direction and canted out-of-plane by 30° relative to the [001] direction) in our gazing incidence geometry, we can probe the in-plane $d_{x^2-y^2}$ orbitals or primarily the out-of-plane d_{z^2} orbitals of the tetragonal CuO film, respectively.

In fig. 5, we show X-ray absorption spectra for the tetragonal CuO films at the Cu $L_{2,3}$ edges with the $\boldsymbol{E}$ vector aligned in-plane or canted out-of-plane. The peaks at the Cu $L_{2,3}$ edges (*i.e.* at about 930 and 950 eV) correspond to transitions from the Cu $2p_{3/2}$ to Cu $3d$ and Cu $2p_{1/2}$ to Cu $3d$ orbitals, respectively. These transitions are commonly referred to as $2p^6 3d^9 \rightarrow 2p^5 3d^{10}$, where an electron from the Cu $2p$ orbital is promoted to the $3d$ orbital after absorbing a photon [23–25]. We observe a strong dependence of the spectral intensity on the polarization direction with a higher absorption when $\boldsymbol{E}$ is aligned in-plane compared to when it cants out of plane.

The observed large asymmetry of 57.1% (asymmetry = difference of the X-ray absorption signal obtained for $E \perp c$-axis and $E \parallel c$-axis at the L_3 edge divided by the sum) in the spectral intensity gives direct evidence that most of the Cu sites have holes occupying the $d_{x^2-y^2}$ orbital similar to what has been demonstrated for tetragonal $SrCuO_2$ and $La_{1.85}Sr_{0.15}CuO_4$ having closely the same degree of asymmetry. This is unlike the case for the monoclinic phase of CuO [26] or the theoretically predicted hypothetical tetragonal phase with $c/a < 1$ [5,6,27], where the hole is reported to occupy the $e_g d_{z^2}$ orbital. In essence, the results of polarized XAS in relation to the hole occupation at Cu site is in agreement with the discussion based on tetragonal crystal field splitting of the d orbital energy levels as sketched in fig. 1 and hence corroborates the tetragonal structure of CuO with $c/a > 1$.

Conclusions. – We have successfully synthesized tetragonal ultrathin CuO films by a pulsed laser deposition method, imposing epitaxial strain from the STO substrate. The structural characterization during the growth (by RHEED) and after growth (by STEM) unequivocally demonstrate the existence of a tetragonal phase of CuO. Specifically, the findings based on STEM directly reveal that the unit cell of ultrathin CuO layers is elongated along the c-axis with $c/a \sim 1.34$ and has a Cu-O-Cu bond angle, $\varphi = 180 \pm 2$ degree. A combination of ABF and ADF imaging has been used to directly visualize the positions of the heavier (Cu) and the lighter (O) elements, respectively. Structural findings are complemented with polarized XAS experiments that clearly demonstrate that the hole state at the Cu site has a $3d_{x^2-y^2}$ orbital characteristic which is different from the case of bulk monoclinic CuO; where the hole is localized in the $3d_{z^2}$ orbital. Our direct demonstration for the existence of a tetragonal CuO will encourage experiments to probe the associated electronic structure and magnetic state in this novel phase, and also will trigger doping experiments in the quest for high-T_c superconductivity.

$$* * *$$

REFERENCES

[1] Shimizu T., Matsumoto T., Goto T., Yoshimura K. and Kosuge K., *J. Phys. Soc. Jpn.*, **72** (2003) 2165.

[2] Kimura T., Sekio Y., Nakamura H., Siegrist T. and Ramirez A. P., *Nat. Mater*, **7** (2008) 291.

[3] Kastner M. A., Birgeneau R. J., Shirane G. and Endoh Y., *Rev. Mod. Phys.*, **70** (1998) 897.

[4] Rocquefelte X., Schwarz K. and Blaha P., *Sci. Rep.*, **2** (2012) 759.

[5] Chen X., Fu C. L., Franchini C. and Podloucky R., *Phys. Rev. B*, **80** (2009) 094527.

[6] Peralta G., Puggioni D., Filippetti A. and Fiorentini V., *Phys. Rev. B*, **80** (2009) 140408(R).

[7] Bednorz J. and Muller K., *Rev. Mod. Phys.*, **60** (1988) 585.

[8] Grant P. M., *J. Phys.: Conf. Ser.*, **129** (2008) 012042.

[9] Siemons W. *et al.*, *Phys. Rev. B*, **79** (2009) 195122.

[10] Mattheiss L. F., *Phys. Rev. B*, **5** (1972) 290.

[11] Terakura K., Oguchi T., Williams A. R. and Kübler J., *Phys. Rev. B*, **30** (1984) 4734.

[12] Harrison W. A., *Phys. Rev. B*, **76** (2007) 054417.

[13] Fischer G. *et al.*, *Phys. Rev. B*, **80** (2009) 014408.

[14] Ashrink S. and Norrby L. J., *Acta Crystallogr.*, **26** (1970) 8.

[15] Yang B., Thurston T., Tranquada J. and Shirane G., *Phys. Rev. B*, **39** (1989) 4343.

[16] Scagnoli V. *et al.*, *Science*, **332** (2011) 696.

[17] Shimizu T., Matsumoto T., Goto A. and Rao C. T. V., *Phys. Rev. B*, **68** (2003) 224433.

[18] Rosenauer A. and Schowalter M., *Microscopy of Semiconducting Materials 2007, Proceedings of the 15th Conference, 2–5 April 2007, Cambridge, UK, Springer Proceedings in Physics*, Vol. **120** (Springer) 2008, p. 169.

[19] Ghijsen J. *et al.*, *Phys. Rev. B*, **38** (1988) 11322.

[20] Hartel P., Rose H. and Dinges C., *Ultramicroscopy*, **63** (1996) 93.

[21] Findlay S. D. *et al.*, *Appl. Phys. Lett.*, **95** (2009) 191913.

[22] Findlay S. D. *et al.*, *Ultramicroscopy*, **110** (2010) 903.

[23] Chen C. T. *et al.*, *Phys. Rev. Lett.*, **68** (1992) 2543.

[24] Sarma D. D. *et al.*, *Phys. Rev. B*, **37** (1988) 9784.

[25] Aruta C. *et al.*, *Phys. Rev. B*, **78** (2008) 205120.

[26] Filippetti A. and Fiorentini V., *Phys. Rev. Lett.*, **95** (2005) 086405.

[27] Himmetoglu B., Wentzcovitch R. M. and Cococcioni M., *Phys. Rev. B*, **84** (2011) 115108.